3D Imaging of Tapetal Mitochondria Suggests the Importance of Mitochondrial Fission in Pollen Growth[1][OPEN]

Pei-Ying Chen,[a,2] Chia-Chen Wu,[a,2] Chung-Chih Lin,[b] Wann-Neng Jane,[c] and Der-Fen Suen[a,d,3,4]

[a]Agricultural Biotechnology Research Center, Academia Sinica, Taipei 11529, Taiwan
[b]Department of Life Sciences and Institute of Genome Sciences, National Yang-Ming University, Taipei 11221, Taiwan
[c]Institute of Plant and Microbial Biology, Academia Sinica, Taipei 11529, Taiwan
[d]Biotechnology Center, National Chung-Hsing University, Taichung 40227, Taiwan

ORCID ID: 0000-0002-4868-8284 (D.-F.S.).

Mitochondrial fission occurs frequently in plant cells, but its biological significance is poorly understood because mutants specifically impaired in mitochondrial fission do not show obvious defects in vegetative growth. Here, we revealed that the production of viable pollen was reduced in mutants lacking one of the three main proteins involved in mitochondrial fission in Arabidopsis (*Arabidopsis thaliana*), DYNAMIN-RELATED PROTEIN3A (DRP3A)/Arabidopsis DYNAMIN-LIKE PROTEIN2A, DRP3B, and ELONGATED MITOCHONDRIA1 (ELM1). In *drp3b* and *elm1*, young microspores contained an abnormal number of nuclei, and mature pollen had aberrant accumulation of lipids in their coat and an irregular pollen outer wall. Because the formation of the pollen wall and coat is mainly associated with tapetal function, we used 3D imaging to quantify geometric and textural features of cells and mitochondria in the tapetum at different stages, using isolated single tapetal cells in which the in vivo morphology and volume of cells and mitochondria were preserved. Tapetal cells and their mitochondria changed in the volume and morphology at different developmental stages. Defective mitochondrial fission in the *elm1* and *drp3b* mutants caused changes in mitochondrial status, including mitochondrial elongation, abnormal mitochondrial ultrastructure, a decrease in cross-sectional area, and a slight alteration of mitochondrial distribution, as well as a large reduction in mitochondrial density. Our studies suggest that mitochondrial fission is required for proper mitochondrial status in the tapetum and possibly in pollen as well and therefore plays an important role for the production of viable pollen.

Successful production and release of fertile pollen is vital for sexual reproduction. The tapetum is the innermost layer of the anther and encloses the locule where pollen develops. In addition to supplying nutrients for pollen growth, the tapetum synthesizes and transfers pollen outer wall precursors for the formation of the pollen outer wall (Gu et al., 2014; Xu et al., 2014; Shi et al., 2015). From the vacuolated-pollen (VP) stage to the late-tricellular (TC) stage, the tapetum synthesizes and accumulates pollen coat components, including neutral lipid, flavonoid, proteins in elaioplasts, and tapetosomes, and finally undergoes programmed cell death (PCD) to release pollen coat materials onto the pollen (Wu et al., 1997, 1999; Buchanan et al., 2000; Hsieh and Huang, 2007; Li et al., 2012). Therefore, the tapetum plays a key role in pollen development especially in the formation of pollen outer wall and pollen coat. To synthesize, secrete, and transfer materials for pollen growth, the tapetum requires an abundant supply of energy and metabolism.

In nongreen and metabolically active tapetal cells, mitochondria are the major energy source involved in essential metabolism. Cytoplasmic male sterility (CMS), a useful tool for crop breeding, usually results from mitochondrial malfunction in the tapetum due to an abnormal chimeric mitochondrial open reading frame. The chimeric mitochondrial open reading frame is generated not only in the tapetum but also in other cells across the whole CMS plant. However, sporophytic CMS plants usually display no apparent defect in vegetative growth but do have severe defects in the tapetum, resulting in male sterility (Luo et al., 2013; Hu et al., 2014). Tapetal PCD displays characteristics of mitochondrion-mediated

[1]This work was supported by the Academia Sinica, Taiwan, and the Ministry of Science Technology, Taiwan (grant nos. MOST104-2311-B-001-002 and MOST 105-2311-B-001-069).

[2]These authors contributed equally to this article.

[3]Author for contact: suendf@gate.sinica.edu.tw.

[4]Senior author.

The author responsible for distribution of materials integral to the findings presented in this article in accordance with the policy described in the Instructions for Authors (www.plantphysiol.org) is: Der-Fen Suen (suendf@gate.sinica.edu.tw).

D.-F.S. designed the research; P.-Y.C., C.-C.W., C.-C.L., and W.-N. J. performed the research; P.-Y.C. and C.-C.W. performed most of the experiments and contributed equally; D.-F.S. wrote the original article; P.-Y.C., C.-C.W., C.-C.L., W.-N.J., and D.-F.S. reviewed and edited the article

[OPEN]Articles can be viewed without a subscription.

www.plantphysiol.org/cgi/doi/10.1104/pp.19.00183

PCD (Papini et al., 1999). Cytochrome *c* release, a feature of mitochondrion-mediated PCD in animals, was observed during tapetal PCD in CMS lines (Balk and Leaver, 2001; Luo et al., 2013). These findings indicate that proper mitochondrial status is tightly associated with tapetum function and PCD. However, how tapetal mitochondrial status, including mitochondrial morphology, volume, number, and distribution, is altered during pollen development remains elusive.

Mitochondrial morphology is linked to cell energy and metabolic requirements as well as cell fate. To maintain the basic intracellular energy requirement and metabolism, and to respond to different cell conditions, mitochondrial amount and morphology need to be tightly controlled in cells (Scott and Logan, 2011; Rose and Sheahan, 2012; Mishra and Chan, 2016). The formation of dynamic mitochondrial networks in cells is regulated by the fusion and fission machinery. In plants, several proteins are involved in mitochondrial fission; among them, dynamin and dynamin-related proteins play a central role (Arimura, 2018). In Arabidopsis, DYNAMIN-RELATED PROTEIN 3A (DRP3A)/Arabidopsis DYNAMIN-LIKE PROTEIN2A, DRP3B/Arabidopsis DYNAMIN-LIKE PROTEIN2B, ELONGATED MITOCHONDRIA1 (ELM1), PEROXISOMAL and MITOCHONDRIAL DIVISION FACTOR1, MITOCHONDRIAL DIVISION FACTOR 2, and FISSION1A and FISSION1B are involved in mitochondrial fission (Arimura and Tsutsumi, 2002; Arimura et al., 2004, 2008; Logan et al., 2004; Mano et al., 2004; Scott et al., 2006; Fujimoto et al., 2009; Aung and Hu, 2012). DRP3A and DRP3B belong to the dynamin family and are localized to mitochondria and peroxisomes (Arimura and Tsutsumi, 2002; Arimura et al., 2004; Logan et al., 2004; Mano et al., 2004; Fujimoto et al., 2009). DRP3A and DRP3B are functionally redundant in mitochondrial fission but have distinct roles in peroxisome division (Fujimoto et al., 2009). Plant-specific protein ELM1 (NETWORK1) was the first plant- and mitochondrial-specific fission protein discovered (Logan et al., 2003; Arimura et al., 2008; Logan, 2010). ELM1 interacts with DRP3A and perhaps DRP3B to recruit them to the mitochondrial fission sites (Arimura et al., 2008). However, the importance of mitochondrial fission in plants is unknown because the mitochondrial fission mutants with elongated mitochondria investigated to date do not display obvious defects in general plant growth.

To better understand the importance of mitochondrial fission in pollen development, we investigated *drp3a*, *drp3b*, and *elm1* mutants and observed that these mutants had elongated mitochondria in the tapetum and developing pollen, and a reduced pollen number. Furthermore, using 3D imaging of single tapetal cells, we were able to quantify the volume and morphology of tapetal cells and whole mitochondrial network as well as the geometric and textural features of mitochondria in wild-type and mitochondrial fission mutants. Our results showed that the volume and shape of tapetal cells and mitochondrial amount and morphology in the tapetum changed as pollen developed, and defects in mitochondrial fission caused reductions in pollen production possibly by disrupting mitochondrial status in the tapetum and pollen.

RESULTS

Mutants Lacking DRP3A, DRP3B, and ELM1 Showed Decreased Production of Viable Pollen

In agreement with previous studies (Arimura et al., 2008; Fujimoto et al., 2009; Aung and Hu, 2012), we did not detect apparent defects in vegetative growth of null *drp3a*, *drp3b*, and *elm1* mutants. However, shorter siliques, and a reduced number of siliques, were observed in the mutants (Fig. 1, A–E). We further examined the total number of viable and aborted pollen per anther using Alexander staining (Fig. 1, F, G, J, K, N, and O; Supplemental Fig. S1, A–C). Under normal light condition ($\sim$110 μmol m^{-2} s^{-1}), all mutants displayed a significant increase (3% to 6%) in aborted pollen and a decrease of $\sim$30% in total pollen number per anther, compared with wild type (Fig. 1, N and O). Expressing *ELM1* driven by its native promoter in an *elm1* mutant background restored the relative total pollen number per anther and the percentage of aborted pollen number to wild-type levels (Supplemental Fig. S2), indicating that reduced pollen production in the *elm1* mutant was caused by the loss of ELM1.

We also examined wild-type and mutant plants that had been grown under normal light conditions ($\sim$110 μmol m^{-2} s^{-1}) during the vegetative stage before being transferred to low light conditions ($\sim$45 μmol m^{-2} s^{-1}) after the emergence of inflorescences. In addition to oxidative phosphorylation in mitochondria, carbohydrate breakdown such as glycolysis is an alternative way to generate ATP in nongreen tissues. In plants, carbohydrate is mainly produced from photosynthesis and transported to sink tissue such as the tapetum and pollen. A long period of low-light treatment reduces the activity of PSII and the content of photosynthetic pigments (Dong et al., 2014; Zhang et al., 2016), which may reduce carbohydrate supply and make plants rely more on mitochondrial function. After transfer to low light, the percentage of aborted mature pollen did not change in the wild type compared with that in plants remaining in normal light, but increased $\sim$2-fold in the mutants (Fig. 1, H, I, L, M, and O; Supplemental Fig. S1, D–F). In addition, the total number of pollen per anther was reduced 20% in wild type but was increased 40% in the mutants (Fig. 1N). These results indicated that mitochondrial fission is important for the production of viable pollen, especially under low light conditions. Because ELM1 and DRP3B are known to primarily affect mitochondrial division, the following analyses were performed in *elm1* and *drp3b* mutants.

Mitochondria and Pollen in the Fission Mutants Showed Defective Morphologies

To verify the alteration of mitochondrial morphology in mitochondrial fission mutants, we analyzed

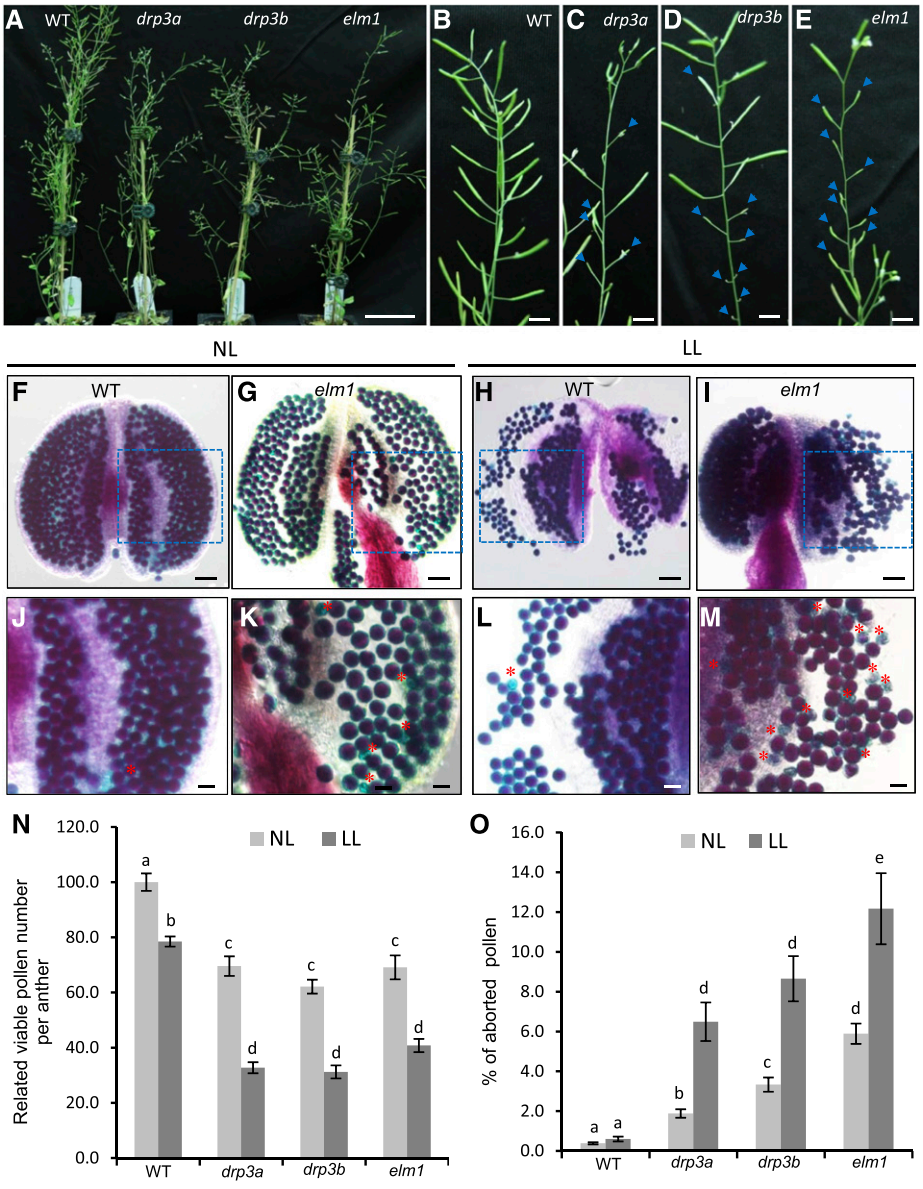

Figure 1. Reproductive growth and pollen production in wild type and mitochondrial fission mutants. A to E, Forty-three-d–old plants grown under normal light conditions, showing whole plants (A) and siliques of wild type (B), *drp3a* (C), *drp3b* (D), and *elm1* (E). Blue arrows indicate abnormal morphology of siliques. F to M, Alexander staining of mature pollen of plants grown under normal (~110 μmol m^{-2} s^{-1}; F, G, J, and K) and low light (~45 μmol m^{-2} s^{-1}; H, I, L, and M) conditions. J to M, Enlargement of the areas enclosed by the dashed boxes in (F) to (I). Red asterisks indicate aborted pollen. N, Relative viable pollen per anther (versus wild type). O, Percentage of aborted pollen. A total of six anthers from three plants (two anthers per plant) was used for each experiment with three biological repeats. All the pollen in each anther was counted. The results are shown as mean ± SE. Statistically significant difference ($P < 0.05$) is indicated by different letters according to Student's *t* test. Scale bars = 5 cm (A); 2 cm (B–E); 50 μm (F–I); 20 μm (J–M). NL, normal light; LL, low light.

mitochondria in the tapetum and pollen in wild type and mutants using transmission electron microscopy (TEM). Our data showed that mitochondria were elongated in both the tapetum and developing pollen in *elm1* and *drp3b* mutants, in contrast to the small and round-shaped mitochondria in wild type (Fig. 2, A–H; Supplemental Fig. S3). At the young microspore (YM) stage, *elm1* but not *drp3b* pollen contained a number of mitochondria that were swollen and had less matrix content and cristae structure (Fig. 2B). Among the elongated mitochondria in the mutant tapetum, some had normal cristae and matrix density (Fig. 2F; Supplemental Fig. S4), whereas others contained vesicle- and vacuole-like structures in the matrix or lower cristae and matrix content (Fig. 2, G and H; Supplemental Fig. S4). To understand which pollen defect is caused by mitochondrial fission deficiency, we first performed Cryo-scanning electron microscopy (Cryo-SEM) to investigate mature pollen from wild type, *elm1*, and *drp3b*, which showed that wild-type pollen had a clear reticule-like outer wall pattern and folded inward to form the "olive" shape (Fig. 3, A, D, and H). However, a portion of the mutant pollen had aberrant structure on the pollen outer wall, and some pollen walls were covered by an overaccumulation of a pollen-coat–like structure on their surface (Fig. 3, B, C, E, G, and I–K). In addition, unlike the olive-shaped pollen in the wild type, a large portion of the pollen in the *elm1* and *drp3b* mutants was round, which may indicate impaired inward folding of pollen.

Normally the pollen outer wall is covered evenly with pollen coat components that are mainly composed of neutral lipids, proteins, and flavonoids, which are synthesized in the tapetum (Wu et al., 1997; Ting et al., 1998; Hsieh and Huang, 2005, 2007). Because we observed abnormal material accumulation on the surface

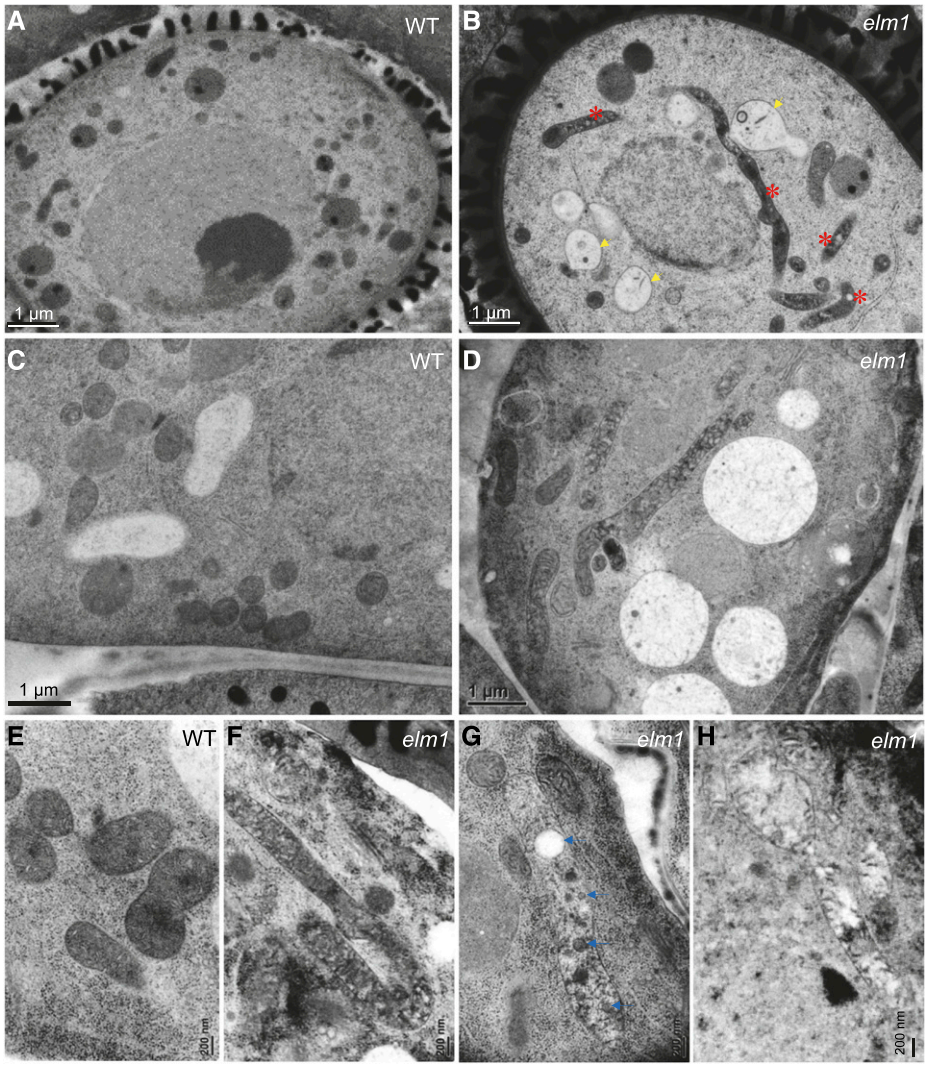

Figure 2. TEM images showing mitochondrial morphology in the tapetum and pollen of wild type (WT) and *elm1*. A to D, Pollen (A and B) and the tapetum (C and D) at the YM stage. E to H, Mitochondria in wild-type tapetum (E); mitochondria with abundant cristae (F), vacuole- and vesicle-like structures (G), and lower cristae and matrix content (H) in *elm1* tapetum. Red asterisks indicate elongated mitochondria. Yellow arrows indicate mitochondria containing less cristae and matrix content. Blue arrows indicate vacuole- or vesicle-like structures in mitochondria. Scale bars = 1 μm (A–D); 200 nm (E–H).

of *elm1* and *drp3b* pollen, more obvious in the *elm1* mutant, we analyzed neutral lipids on the surface (Fig. 4, A–F) and in the interior (Fig. 4, G–L) of wild-type and *elm1* pollen by imaging the optical top and cross-view of mature pollen that were stained with Nile Red, a neutral lipid-staining dye. Wild-type and *elm1* pollen did not show an obvious difference in the amount and size of neutral lipid droplets in the pollen interior (Fig. 4, G–L). However, unlike wild-type pollen in which neutral lipids were evenly distributed in the cavities of the pollen outer wall (Fig. 4, A–C and G–I), neutral lipids formed big clumps on the surface of *elm1* pollen (Fig. 4, D–F and J–L). The results indicated that in mitochondrial fission mutants, the formation of both pollen outer wall and pollen coat were impaired, implying a disruption of tapetal function.

Because the total pollen number per anther was reduced in the mutants, we reasoned that mutant pollen had defects leading to degeneration before pollen maturation. To reveal the defect in developing pollen in the mutants, we analyzed YMs using light microscopy, 4',6-diamidino-2-phenylindole (DAPI) staining, and TEM. Each wild-type YM contained one nucleus (Fig. 5, A, D, G, and J), but in the mutants, some YMs possessed two nuclei (Fig. 5, B, C, E, and F), whereas others lacked a nucleus (Fig. 5, H, I, K, and L), suggesting that defects in mitochondrial fission affect nuclear number in YMs. Mitochondria are the major ATP-generating organelles in pollen, and thus we analyzed ATP content in mature pollen from wild type and *elm1*, reasoning that the *elm1* mutant would possibly have a stronger influence on metabolism because it showed more severe defects in mitochondrial morphology and pollen development. However, ATP content (pM/μg protein) in *elm1* was similar to that in wild type (Supplemental Fig. S5). These results suggested that defects in mitochondrial fission disrupted tapetal function and nuclear number in developing pollen but did not affect ATP content in mature pollen.

Establishment of 3D Imaging of Tapetal Cells and Mitochondria

Because tapetal function is important for the composition of the pollen outer wall and the pollen coat,

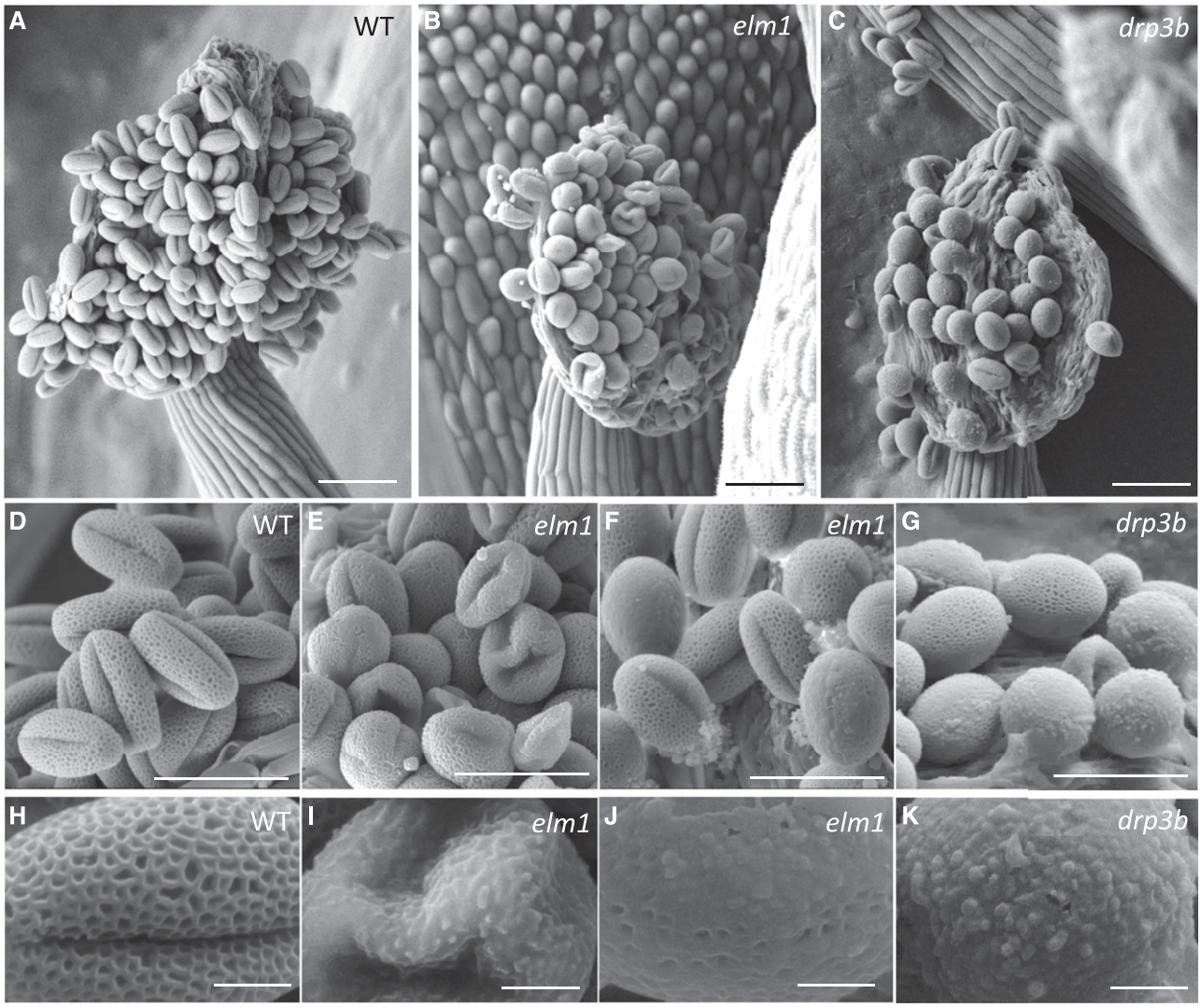

Figure 3. Cryo-SEM of pollen of wild type (WT) and mutants. A to C, Dehiscent anthers. D to G, Mature pollen. H to K, Surface of mature pollen. Scale bars = 50 μm (A–C); 30 μm (D–G); 5 μm (H–K).

which were obviously affected in *elm1* and *drp3b* mutants, we used tapetal cells to investigate how defective mitochondrial fission disturbs mitochondrial status, including the morphology, number, volume, and distribution in cells. To this end, we generated transgenic Arabidopsis plants expressing tapetal specific mitochondrion-targeted GFP (mito-GFP), using the tapetum-specific promoter of *At5g62080* that is expressed from the pollen mother cell (PMC) to the TC stage (Huang et al., 2013). Confocal images of anthers from transgenic plants showed strong and specific expression of mito-GFP in the innermost layer, which lacks the fluorescence signal of chlorophyll (Fig. 6, A–C), indicating that mito-GFP was specifically expressed in the tapetum, the only layer of the anther wall layers known to be void of differentiated chloroplasts.

Taking advantage of the fact that there is a relatively loose connection among tapetal cells and between the tapetum and the adjacent wall layer (Owen and Makaroff, 1995), we used fixatives to preserve in vivo features of cells and then separated tapetal cells from other anther wall layers to obtain single tapetal cells. The isolated tapetal cells are relatively thin and transparent, thus facilitating the acquisition of high-quality images of organelles and the analysis of their detailed geometric and textural features. In transgenic lines, mito-GFP was detected in the double-nuclei tapetal cells (Fig. 6, D and F; Supplemental Movie S1) and colocalized with the mitochondrion-specific dye MitoTracker red (Supplemental Fig. S6), demonstrating the targeting of mito-GFP to tapetal mitochondria. We also stained the entire single tapetal cells with propidium iodide (PI; Fig. 6G; Supplemental Movie S2), which is a fluorescence dye for plant cell walls and can only penetrate dead cells. The PI and mito-GFP fluorescence signals in single tapetal cells were captured and later

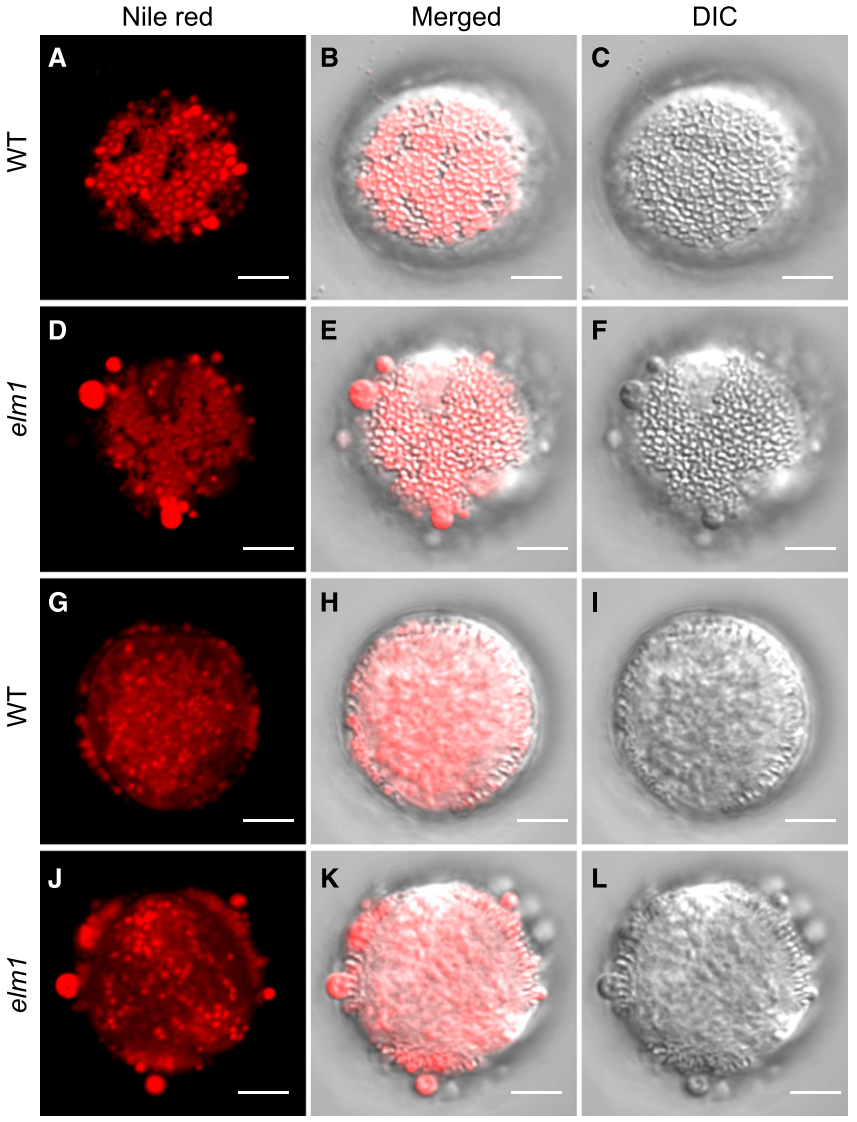

Figure 4. Nile red staining of wild-type (WT) and *elm1* mature pollen. Mature pollen was stained with Nile red, a dye specifically staining neutral lipids. Images were acquired and processed by a model no. LSM780 plus ELYRA confocal microscope (Zeiss). The optical top views (A–F) and optical cross views (G–L) of mature pollen are displayed to show the distribution of neutral lipids in and on pollen. B, E, H, and K, Merged images of Nile red fluorescence (from A, D, G, and J) and DIC (from C, F, I, and L). Scale bars = 5 μm.

used for 3D imaging of tapetal cells and mitochondria. Finally, we established a link among the longitudinal size of flower buds, pollen stages, and the anther stages classified by Sanders et al. (1999) by differential interference contrast (DIC) microscopy, DAPI staining, and TEM (Supplemental Fig. S7) to facilitate routine collection of anthers at different developmental stages.

Tapetal Cells and their Mitochondria Changed in the Volume and Morphology at Different Developmental Stages

It was unclear how the tapetum alters its cell volume to coordinate with pollen growth at different stages and the process of tapetal PCD. To this end, we analyzed features of tapetal cells, using single tapetal cells isolated from seven developmental stages: PMC, meiosis, tetrad, YM, VP, binucleate (BN), and TC. PI-stained cells were imaged by confocal microscopy, and the volume and shape of tapetal cells were quantified using the software IMARIS (Bitplane; Chen et al., 2016) and MicroP 3D, a homemade MatLab-based software (The MathWorks; Fig. 7). During pollen development, the volume of tapetal cells increased >3-fold from the PMC to the VP stage, after which it remained unchanged at the BN and TC stages (Fig. 7, A and B). To reveal changes in tapetal shapes at different stages, the major, first minor, and second minor axes (*y*-, *x*-, and *z*-axes, respectively, in the first 3D image of Fig. 7A) of tapetal cells were measured. Except from the meiosis to tetrad stage, the ratio of the major and first minor axis of tapetal cells did not change during development (Fig. 7, A and C), suggesting that during tapetal cell enlargement, a similar ratio of major to first minor axis was mostly maintained. The ratio of major to second minor axis of tapetal cells was not changed from PMC to YM but increased at the VP and BN stages (Fig. 7D), indicating that the thickness (*z*-axis) of tapetal cells was reduced at the late stage, which agrees with results

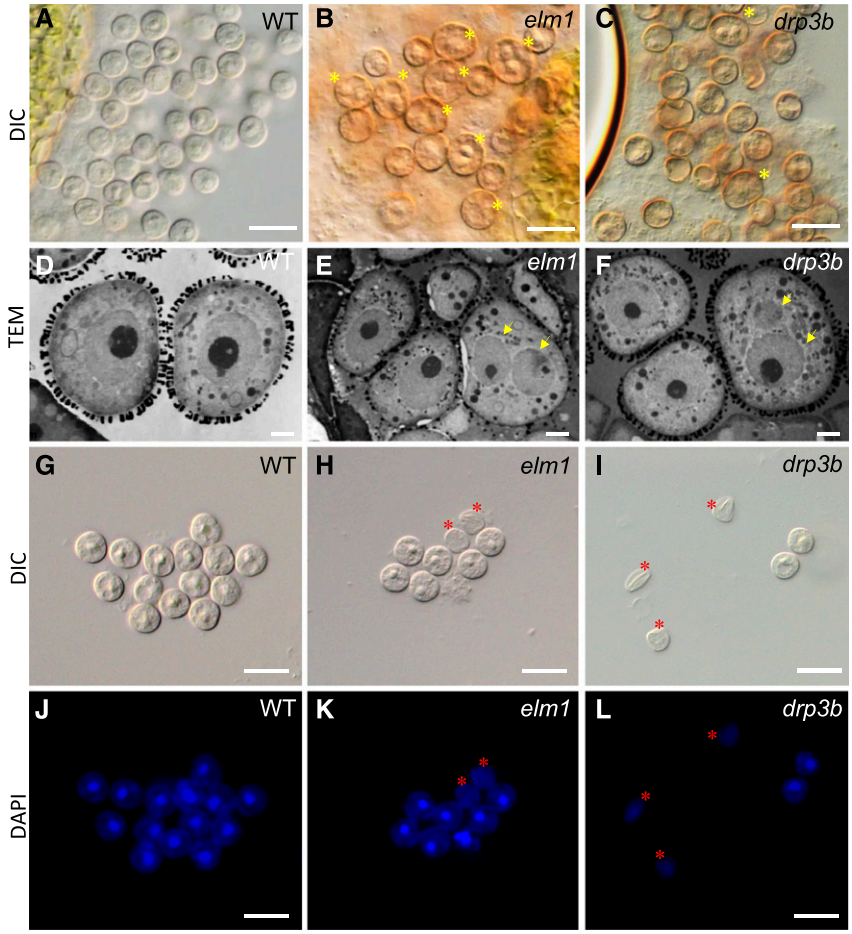

Figure 5. Morphology of YM-stage pollen of plants grown under normal light condition. DIC (A–C and G–I), TEM (D–F), and images of pollen stained by DAPI (J–L). Yellow asterisks in (B) and (C) show microspores with double nuclei. Yellow arrows in (E) and (F) point to nuclei. Red asterisks in (H), (I), (K), and (L) show the microspores lacking a nucleus. Scale bars = 20 μm (A–C, G–L); 2 μm (D–F).

from the IMARIS-mediated reconstruction of 3D morphology of tapetal cells (Fig. 7A). These results showed that at the BN and TC stages, instead of enlarging cell volume, the tapetum reduced its thickness—probably to increase the area facing the locule for the expansion of locule space.

We next determined the status of tapetal mitochondria during pollen development in wild-type plants. Mito-GFP signals of single tapetal cells at the seven stages as described above were imaged and quantified for mitochondrial volume and features (Fig. 8). Total mitochondrial volume in each tapetal cell increased

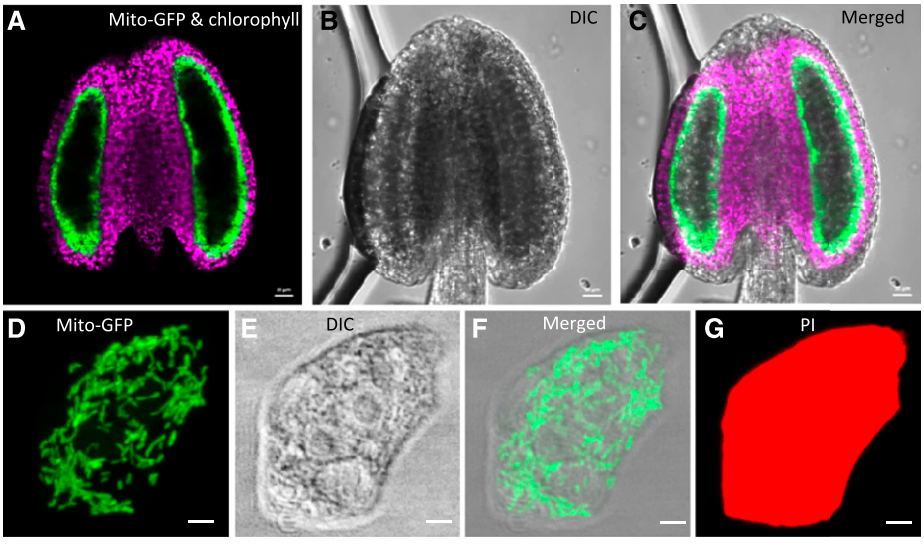

Figure 6. Expression of mito-GFP in tetrad-stage anthers and tapetal cells from Arabidopsis plants expressing tapetum-specific mito-GFP. A to C, Single-section images of an anther. D to G, Projected images of mitochondria in a single tapetal cell. Mito-GFP and chlorophyll fluorescence (A), DIC (B), and merged (C) images of an anther. Mito-GFP fluorescence (D), DIC (E), merged (F), and PI (G) images of a tapetal cell. GFP signal is green, chlorophyll signal is purple, and PI signal is red. Scale bars = 20 μm (A–C); 2.5 μm (D–G).

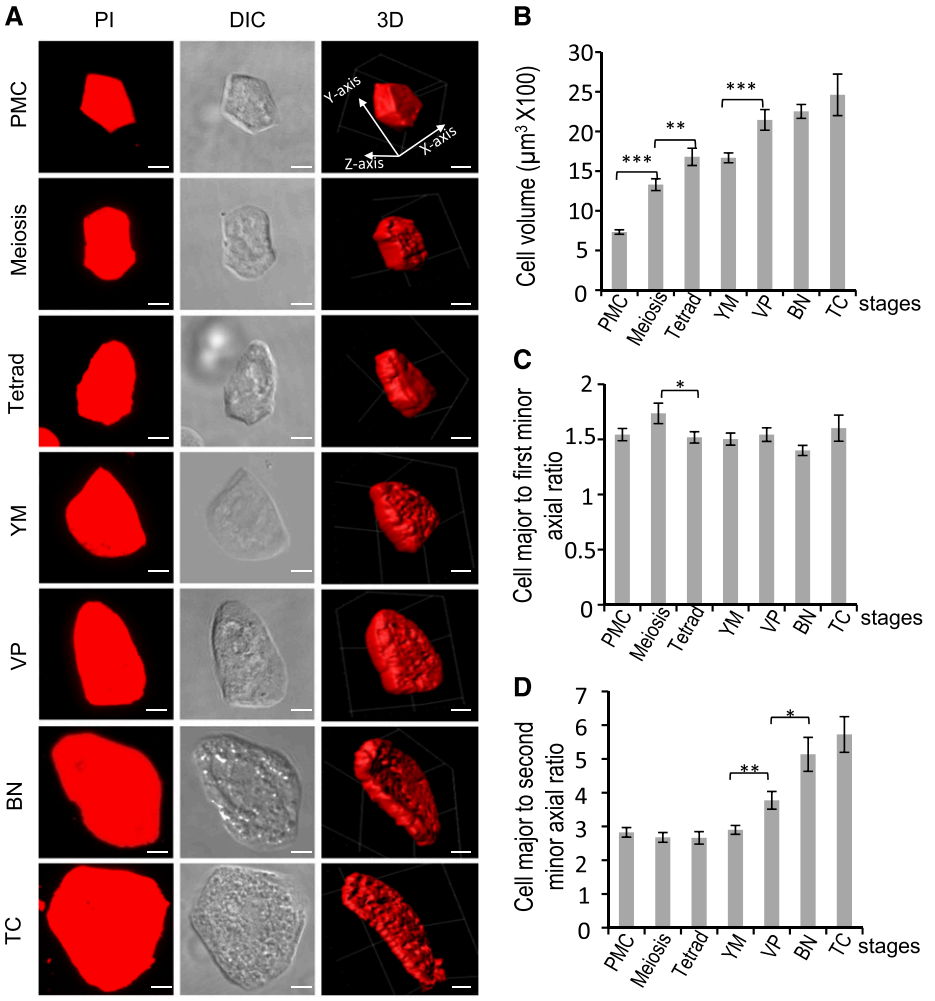

Figure 7. Numerical analysis of cell morphology of tapetal cells in wild type. A, Z-projected images of PI-stained tapetal cells at different stages. Three-dimensional image stacks of cells were acquired by confocal microscopy and reconstructed by the software IMARIS. Scale bars = 5 μm. The PI micrographs were further used for numerical analysis of cell morphology, including volume (B) and shape (C and D). For quantification of cell morphology, length of axes of the cell was calculated. The *y*-, *x*-, and *z*-axes are the major, first minor, and second minor axes, respectively. B to D, Morphological changes of cell morphology of wild-type cells at different stages. Cell number quantified at each stage per experiment was ≥19. Three biological repeats were performed ($n = 3$). Results are shown as mean ± SE. Statistically significant difference (*$P < 0.05$; **$P < 0.01$; ***$P < 0.001$) is analyzed by Student's *t* test.

>6-fold from the PMC to the VP stages and reduced ~3-fold from the VP to the TC stages (Fig. 8D). Given that cell size affects cellular energy demand, which is positively linked to mitochondrial amount, we examined whether the change in total mitochondrial volume in tapetal cells simply reflects the enlargement of tapetal cell volume, by calculating mitochondrial density in the tapetum (mitochondrial volume per unit volume of tapetal cell). Mitochondrial density increased ~2-fold from the PMC to the YM stage; was unchanged at the VP stage; and decreased 2.7-fold from the VP to the TC stage (Fig. 8E). We reasoned from these data that the alteration of mitochondrial amount in the tapetum is not only due to the change of tapetal cell volume but also to other cellular demands.

Remarkably, our 3D imaging of mito-GFP revealed mitochondrial fragmentation in tapetal cells at the BN and TC stages (Fig. 8, A and B). The geometric and textural features of tapetal mitochondria were further extracted using MicroP 3D to quantitatively analyze the size, number, and cross section of tapetal mitochondria (Fig. 8, C, and F–H). Based on the extracted morphological features, tapetal mitochondria were classified into six subtypes: fragments, lumps, simple tubules, branched tubules, small reticulum, and large reticulum, shown in representative tapetal cells in Figure 8C. At the BN and TC stages in tapetal cells, the percentage was increased for fragments, lumps, and short tubule subtypes (Supplemental Fig. S8, A–C), but largely decreased for the small and large reticulum subtypes (Supplemental Fig. S8, D and E). The number of mitochondria remained statistically unchanged from the PMC to the VP stage but was increased at the BN and TC stages (Fig. 8F). The mean value of individual mitochondrial size (volume) was increased from PMC to meiosis and remained the same from the meiosis to the VP stage. Subsequently mitochondrial size was dramatically decreased at the BN and TC stages (Fig. 8G). Compared to the VP stage, tapetal mitochondrial volume was decreased but total mitochondrial number was dramatically increased at the BN and TC stages (Fig. 8, D and F). Taken together, these results indicated that mitochondrial size in the tapetum was decreased at the BN and TC stages. In addition, individual mitochondrial size (volume) was smaller at the TC than the BN stage, and the area of the cross section of the mitochondrial skeleton, which represents the diameter of mitochondria, did not change at the BN stage but

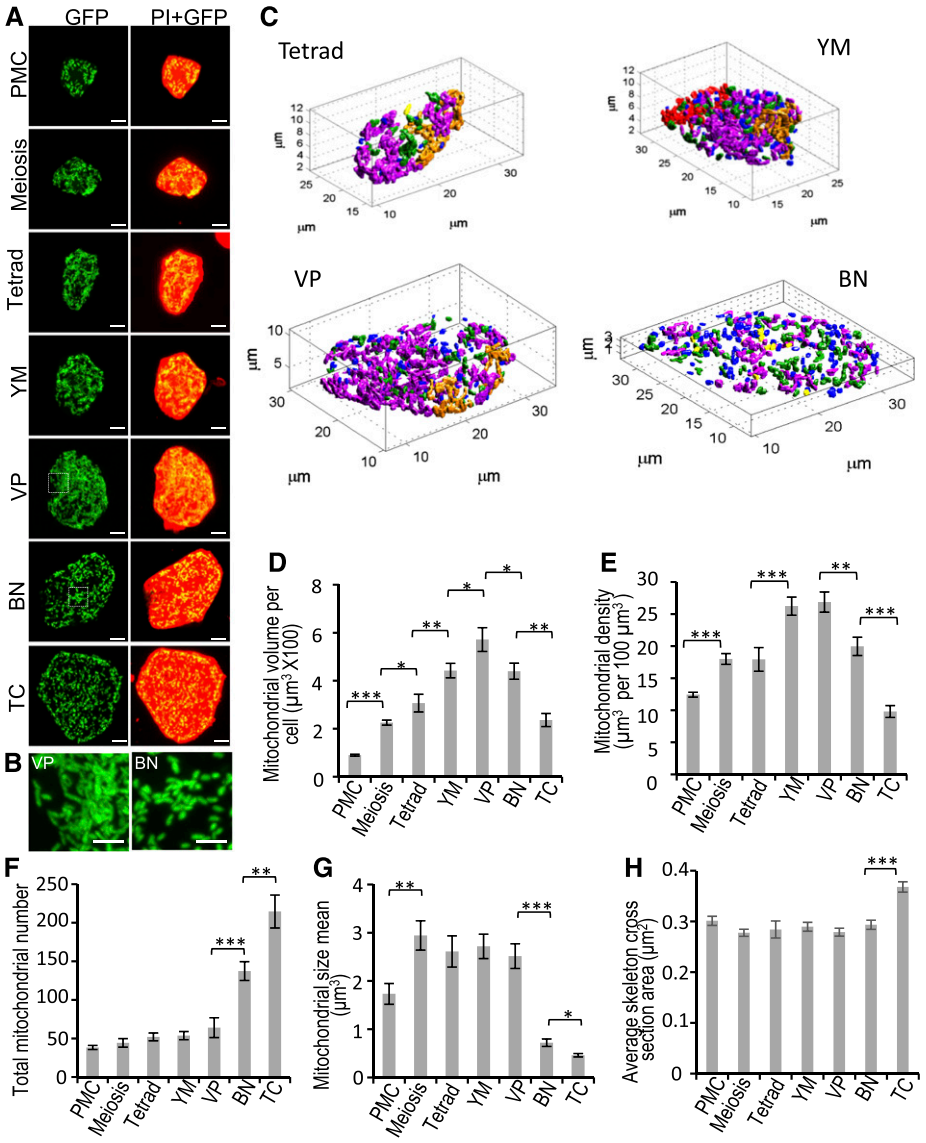

Figure 8. Morphological changes of mitochondria in wild-type tapetum during development. Individual tapetal cells expressing mito-GFP at different stages were separated from anthers and stained with PI. A, Z-projected images of mito-GFP and PI of individual cells. PI signal is red, and mito-GFP signal is green. Scale bars = 5 μm. B, Magnified image of tapetal mitochondria enclosed in the box in (A). Scale bars = 2.5 μm. C, Three-dimensional numerical mitochondrial morphological analysis performed by microP 3D. D to H, Mitochondria of tapetal cells were classified into six mitochondrial subtypes: fragments (blue), lumps (yellow), simple tubules (green), branched tubules (light purple), small reticulum (gold), and large reticulum (red). Four tapetal cells at the tetrad, YM, VP, and BN stages are displayed to demonstrate mitochondria of six subtypes. Total mitochondrial volume per tapetal cell (D), mitochondrial density (E, with mitochondrial volume/tapetal volume), total mitochondrial number (F), mitochondria mean size (G), and average skeleton cross-section area of tapetal mitochondria (H) was measured and shown as mean ± SE ($n \geq 10$/stage; $n = 3$). Statistically significant difference (*$P <$ 0.05; **$P < 0.01$; ***$P < 0.001$) is analyzed by Student's *t* test.

significantly increased at the TC stage (Fig. 8H), indicating that mitochondria become swollen at the TC stage.

Tapetal Mitochondria in the Fission Mutants Altered in Amount and Size

Earlier in this study, we showed that lack of DRP3B and ELM1 affected the formation of pollen wall and pollen coat, processes that rely on proper tapetal function. To investigate whether and how mitochondrial status is altered in *drp3b* and *elm1* tapetum, we expressed tapetum-specific mito-GFP in the mutants and analyzed tapetal mitochondria at different developmental stages. In the tapetum of *drp3b* and *elm1*, mitochondria became elongated, and mitochondrial fragmentation at the BN stage was inhibited (Fig. 9, A–C; Supplemental Fig. S9). Quantification of 3D images of tapetal mitochondria revealed that total amounts of mitochondria (volume) per cell was significantly decreased in both *drp3b* and *elm1* mutants from the YM to the BN stages (Fig. 9D). The mean size of tapetal mitochondria (the average of individual mitochondrial volume) at most of the stages was increased slightly in *drp3b* and dramatically in *elm1* (Fig. 9E). Interestingly, not only wild type and *drp3b* but also *elm1* displayed a statistically significant reduction in mitochondrial size at the BN stage (Fig. 9E), indicating that mitochondrial fission is not completely blocked in *elm1* tapetum. In addition, mitochondrial number in both mutants was decreased (Fig. 9F), which negatively correlated with the increase of mitochondrial size. In *elm1* and *drp3b*, tapetal mitochondria were elongated, increased in the long axis (Fig. 9, B and C; Supplemental Fig. S9) with decreases in the average area of the mitochondrial skeletal cross section (Fig. 9G). During development, wild type, *elm1*,

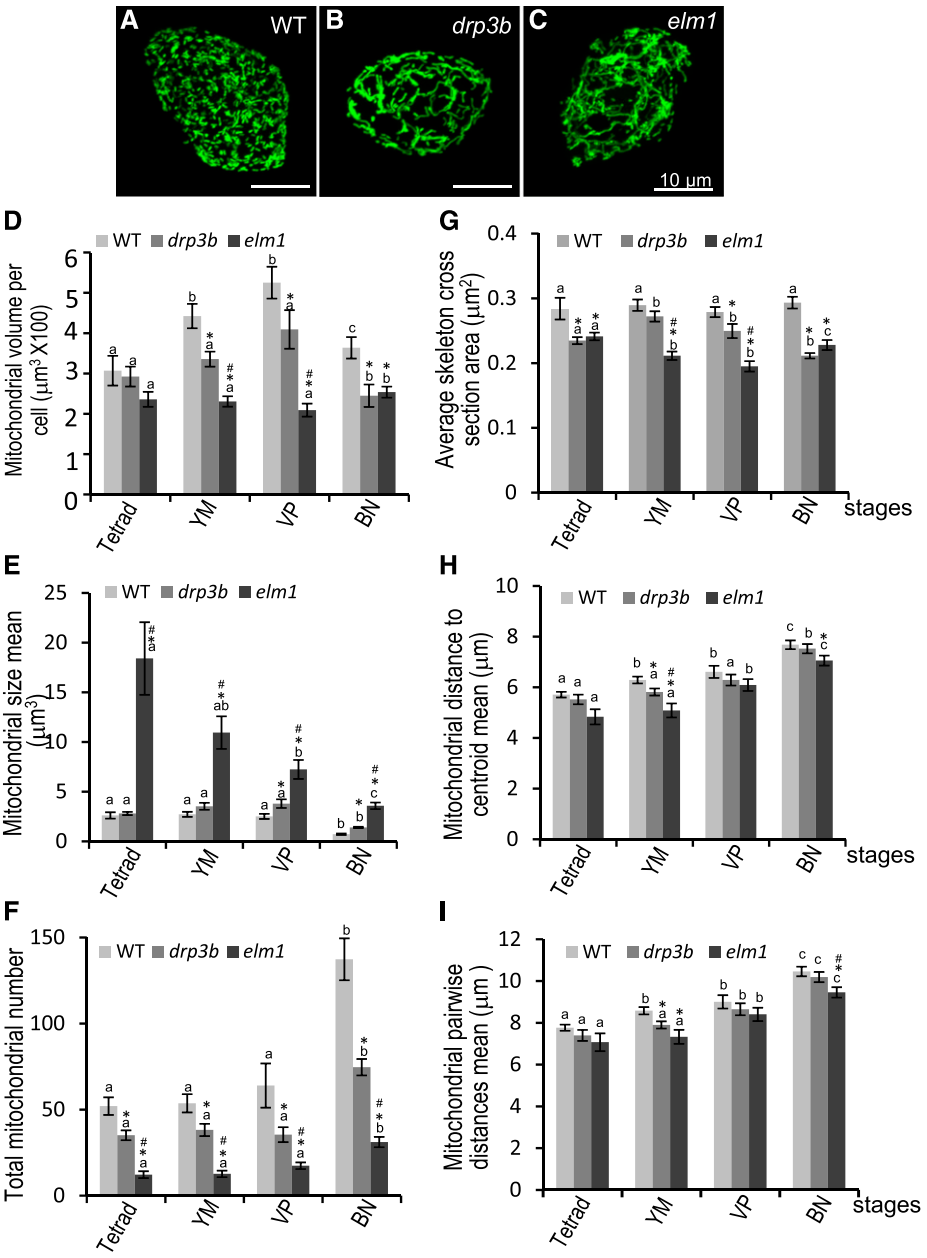

Figure 9. Tapetal mitochondria in wild-type (WT), *drp3b*, and *elm1* mutants. A to C, Confocal images of mitochondria in a BN-stage tapetal cell expressing mito-GFP. Scale bars = 10 μm. D, Quantification of total mitochondrial volume per tapetal cell. E, Mitochondrial size (the volume of individual mitochondria). F, Total mitochondria number. G, The average skeleton cross-section area of tapetal mitochondria. H, Mitochondrial distance to centroid of the whole mitochondrial population in cells. I, Mean of mitochondrial pairwise distance. At least 20 tapetal cells of each genotype at each stage were quantified from three biological experiments. The results are shown as mean ± SE. The statistically significant difference ($P < 0.05$) between stages of each genotype is indicated by a different letter according to Student's *t* test. Within a stage, significant difference ($P < 0.05$) of mutants versus wild type and between two mutants are labeled with "*" and "#", respectively.

and *drp3b* all displayed a gradual increase in the distance from mitochondria to the centroid (Fig. 9H) and the distance between mitochondria (Fig. 9I), which may have been a response to the increase in tapetal cell volume. Compared with the wild type, the distance from mitochondria to the centroid and the distance between the two mitochondria in the mutants showed no significant difference at the tetrad and VP stages but a slight decrease at the YM and BN stages (Fig. 9, H and I). These results demonstrated that defects in mitochondrial fission not only caused mitochondrial elongation and decreases in mitochondrial number but also a reduction of total mitochondrial volume, and a slight change in mitochondrial distribution in the tapetum.

DISCUSSION

Defects in Mitochondrial Fission Affects Tapetal Function and Pollen Development

In this study, a subset of *elm1* pollen showed a disconnected pattern of their outer wall, which is often observed in mutants with defects in the synthesis or the transfer of sporopollenin, the pollen outer wall precursor, in the tapetum (Grienenberger et al., 2010; Kim et al., 2010; Quilichini et al., 2010; Shi et al., 2011; Chen et al., 2017). In addition, we observed clumps of neutral lipids on the surface of mutant pollen, which may be due to aberrant lipid synthesis and accumulation in the tapetum or abnormal outer wall that is disrupted in the storage of pollen coat components. Sporopollenin and

neutral lipid, a component of the pollen coat, are synthesized from fatty acids in the tapetum, and these processes require a large supply of energy and precursor (Wu et al., 1997; Ting et al., 1998; Hsieh and Huang, 2005, 2007; Ariizumi and Toriyama, 2011). Mitochondria are the main energy source and produce acetyl-CoA, the precursor of fatty acid biosynthesis as well as the product of β-oxidation that is important for lipid utility in cells. Our 3D imaging and quantification of mitochondria in single tapetal cells revealed that defects in mitochondrial fission significantly affect mitochondrial size and total mitochondrial amount and slightly affect mitochondrial distribution. The change of mitochondrial status in mitochondrial fission mutants likely disrupts energy supply from, and metabolism in, mitochondria, affecting the function of the tapetum in the formation of pollen outer wall and pollen coat.

Mitochondrial number was shown to be dramatically increased in pollen and the tapetum but not in other anther layers during early developmental stages (Lee and Warmke, 1979). In addition, mitochondrial volume in mature pollen is ~4-fold of that at the BN stage (Cai et al., 2015). These results suggest that during pollen development, mitochondrial amount in pollen needs to be adjusted, which relies on mitochondrial fission activity. In this study, we showed that defects in mitochondrial fission impact mitochondrial morphology and nuclear number in developing pollen but did not affect ATP content in mature pollen, suggesting that mitochondrial fission did not play a main role in sustaining ATP content in mature pollen but is required for maintaining proper number of nuclei in developing pollen. It is also possible that disrupting mitochondrial function in developing pollen in the mitochondrial fission mutants contributes to the reduction of viable pollen production.

Mitochondrial Status But Not Cell Volume Changed in the Tapetum during PCD

An increase in mitochondrial function usually reflects a rise in energy demand in cells. Based on the appearance of a high abundance of endoplasmic reticulum, Golgi, and mitochondria in TEM images of the tapetum, it was suggested that the tapetum becomes metabolically active at the tetrad and YM stages (Quilichini et al., 2014). However, in this study, we demonstrated that mitochondrial density in tapetal cells increased not only at the tetrad-to-YM stage but also at the PMC-to-meiosis stage. This suggests that the tapetum might become metabolically active as early as the meiosis stage. In addition, the analysis of TEM images in a previous study showed that at around the BN stage in Arabidopsis, tapetal PCD seems to be initiated and tapetal cells are shrunken (Vizcay-Barrena and Wilson, 2006; Phan et al., 2011; Quilichini et al., 2014). However, we revealed that the tapetum remained a similar volume from the VP to the TC stages, indicating that the tapetal cell volume is not gradually reduced while PCD occurs. In animals, mitochondrial fragmentation facilitates mitochondrial elimination and transport and is associated with the initiation of mitochondrion-mediated PCD (Arnoult, 2007; Suen et al., 2008; Mishra and Chan, 2016). Our geometric and textural analysis of tapetal mitochondria found these organelles to be fragmented at the BN stage, when reduction of mitochondrial amount in tapetal cells and tapetum PCD occur (Vizcay-Barrena and Wilson, 2006; Phan et al., 2011; Quilichini et al., 2014), suggesting that this mitochondrial fragmentation in the tapetum at the BN stage may be related to the reduction of total mitochondrial volume and the early process of PCD in the tapetum. It has been shown that mitochondrial matrix swelling results from the loss of selective permeability of the mitochondrial inner membrane (Zoratti and Szabò, 1995; Green and Reed, 1998; Crompton, 1999). Our finding that mitochondrial swelling occurs at the TC stage implies that the loss of mitochondrial membrane permeability may be a feature of tapetal PCD.

ELM1-Dependent Fission Is Critical for Controlling the Size of Tapetal Mitochondria

DRP3A and DRP3B are functionally redundant in plant mitochondrial fission (Arimura and Tsutsumi, 2002; Arimura et al., 2004; Logan et al., 2004; Mano et al., 2004; Fujimoto et al., 2009; Aung and Hu, 2012). In this study, loss of DRP3B only partially inhibited mitochondrial fission and led to mild increases in mitochondrial size in the tapetum. ELM1 is important for mitochondrial localization of DRP3A, and perhaps DRP3B as well (Arimura et al., 2008). Therefore, loss of ELM1 blocked translocation of both DRP3A and DRP3B into the mitochondria, and thus, dramatically increased mitochondrial size in the tapetum. Our result also indicated that ELM1-dependent mitochondrial fission plays a major role in controlling the size of tapetal mitochondria. However, the reduction of mitochondrial size occurred not only in wild type and *drp3b* but also in *elm1* at the BN stage. Recently ELM1-independent mitochondrial targeting of DRP3A was observed under cold stress conditions (Arimura et al., 2017). Therefore, in the absence of ELM1, ELM1-independent fission mechanisms may participate in the reduction of mitochondrial size in the tapetum. On the other hand, DRP3A and DRP3B are localized to not only the mitochondria but also the peroxisome. Even though the role of DRP3B in peroxisome division seems minor, it cannot be excluded that defects in pollen development in *drp3a* and *drp3b* and the abnormal tapetum function in *drp3b* may be related to partially impaired peroxisome division.

CONCLUSION

In this study, we demonstrated that impaired mitochondrial fission reduced the production of viable pollen and disrupted tapetal function, but did not have an obvious impact on vegetative growth. Therefore,

tapetal function and pollen development seem to be more sensitive to mitochondrial defects, which agrees with data shown in most CMS lines. Isolation of single tapetal cells that preserve their in vivo cell and mitochondrial morphology and volume, followed by 3D imaging-based quantification, led us to the discovery that in wild type, tapetal cells increased in volume from the early to middle stage and change shape at the late stage of development, and that mitochondrial amount and morphology in the tapetum were altered during pollen development. By contrast, defects in mitochondrial fission impaired the adjustment of mitochondrial status in the tapetum and possibly in pollen as well. Our study suggests that mitochondrial fission is critical for tapetal function and pollen development.

MATERIALS AND METHODS

Plant Growth and Materials

Wild-type Arabidopsis (*Arabidopsis thaliana*, ecotype Columbia-0), transgenic lines and mutants were grown at 22°C under ~110 μmol m^{-2} s^{-1} light intensity and a 16-h light/8-h dark cycle. For light treatment, wild-type and mutant plants were grown at 22°C under ~110 μmol m^{-2} s^{-1} light intensity for 21 d, followed by treatment with ~110 μmol m^{-2} s^{-1} (normal) or 45–50 μmol m^{-2} s^{-1} (low) light intensity, respectively. Transfer DNA insertion mutants, SALK_066958 (*drp3a*), SALK_045316 (*drp3b*), and SALK_071234 (*elm1*) were purchased from the Arabidopsis Biological Resource Center. The *elm1* complementation line is a gift from Dr. Shin-Ichi Arimura at The University of Tokyo. The homozygous plants were validated by genotyping. The null mutants were checked by reverse transcription PCR. The mito-GFP was amplified from the plasmid obtained from Dr. Andreas Nebenführ at the University of Tennessee, Knoxville, by a set of primers (mt-GFP-Forward1: 5′-CATGCTTTC ACTACGTCAATCTATAAG-3′, mt-GFP-Forward2: 5′-CTTTCACTACGT CAATCTATAAGATTTTTC-3′, and mt-GFP-Reverse: 5′-TTACTTGTACAG CTCGTCCATGCC-3′). The amplified mito-GFP fragments were cloned into pCambia1304 containing the tapetum-specific promoter of AT5G62080 (Huang et al., 2013), provided by Dr. Anthony H.C. Huang (University of California, Riverside) and Dr. Ming-Der Huang (National Sun Yat-Sen University, Taiwan) between *Nco*I and *Pml*I restriction sites. Transgenic Arabidopsis expressing mito-GFP specifically in the tapetum were generated by floral dipping. Mitochondrial fission mutants expressing tapetum-specific mito-GFP were generated through crossing homozygous mutants and wild-type plants expressing tapetal mito-GFP. Both wild-type and mutants expressing mito-GFP were selected using antibiotics and GFP signals in the anther as well as genotyping.

Analysis of Bud Size, Pollen Stages, and Pollen Viability

Flower buds were collected from primary inflorescences after 3–5 flowers opened. Their size was measured as the length from the tip to the bottom. Using DIC images, DAPI staining, and TEM images, 0.4-, 0.5-, 0.6-, 0.7-, 0.8-, 1.0-, and 1.4-mm buds were identified, respectively, at the PMC, meiosis, tetrad, YM, VP, BN, and TC stages under our growth conditions (Supplemental Fig. S7). Based on the bud size measurement, samples at different stages were collected for experiments. For DAPI staining, fresh anthers were stained in 2 mg/mL of DAPI in phosphate-buffered saline (PBS) for visualization under an Axio Imager Z1 microscope (Zeiss). For Alexander staining, buds with a little white petal emerging out of the sepal were collected, and sepals and petals were opened to make the dye reach anthers more easily. The opened buds were put into Alexander solution and stained overnight. Three buds from three plants (one bud per plant) were stained, and a total of six anthers (two anthers from one bud) were used to quantify total pollen per anther and the percentage of aborted pollen.

TEM of Arabidopsis Anthers

Arabidopsis buds were frozen using a high-pressure freezer (EMPACT2; Leica) at 2000–2050 bar. Freeze substitution was performed in anhydrous acetone (containing 1% [w/v] osmium tetroxide and 0.1% [w/v] uranyl acetate) using a model no. EM AFS2 Freeze Substitution & Low Temperature Embedding System (Leica). Samples were kept consecutively at −85°C for 3 d, −60°C for 1 d, −20°C for 1 d, 0°C for 1 d, and then back to room temperature. Spurr resin or EMBed 812 resin (Electron Microscopy Sciences) was used for infiltration and embedding. Ultrathin sections of 70–90 nm were cut using an Ultracut S Ultramicrotome (Reichert) or an EM UC6 Ultramicrotome (Leica) and collected using 100-mesh copper grids. The sections were then stained with 5% uranyl acetate in 50% methanol for 10 min and 0.4% lead citrate for 4 min, and then observed using a Tecnai Spirit G20 Transmission Electron Microscope (FEI) at 80 KV and the images were taken with an Orius CCD camera (Gatan).

Preparation of Individual Tapetal Cells, PI Staining, and MitoTracker Staining

To separate individual tapetal cells, anthers (from 0.4- to 1.5-mm buds) were fixed in 4% (v/v) paraformaldehyde (cat. no. 15710; Electron Microscopy Sciences) for 30 min under vacuum, and washed twice in 1× PBS buffer for 10 min. Through careful squeezing of paraformaldehyde-fixed anthers on the slide, individual tapetal cells were separated from the anther wall. For analysis of tapetal volume and shape, the isolated individual tapetal cells were stained by 12 mM of PI for 20 min and washed with 1× PBS buffer. To analyze mitochondria in tapetal cells, transgenic Arabidopsis expressing mito-GFP (a gift from Dr. Andreas Nebenführ; Nelson et al., 2007), driven by tapetal specific promoter of type III lipid transfer protein (Huang et al., 2013), was generated. To test the subcellular localization of mito-GFP, anthers expressing mito-GFP were stained with 50 nM of MitoTracker red CMXRos for 30 min in one-half Murashige and Skoog (1/2 MS) medium, and washed with 1/2 MS medium. After staining, anthers were fixed using paraformaldehyde and isolated single tapetal cells, as already described in this paragraph. Tapetal cells stained with PI or MitoTracker red were imaged using a model no. LSM 780 confocal microscope (Zeiss).

Quantification of Volume and Morphology of Cells and Mitochondria in Single Tapetal Cells

For the quantification of tapetal volume and mitochondria, confocal Z-sections of whole tapetal cells were imaged by a model no. LSM 780 confocal microscope with 63×/1.4 oil objectives, 0.11-μm × 0.11-μm × 0.25-μm scaling, 2,048 × 2,048 pixel resolution, 224.92-mm × 224.92-mm image size, 16-bit image format, and 0.6 scanner zoom (Leica). All images were photographed using the same laser and resolution setting. Image stacks of mitochondrial (GFP) and tapetal cell (PI) images were used to measure mitochondrial volume and tapetal volume with the software IMARIS (Bitplane). MicroP 3D, a homemade MatLab-based software (The MathWorks), was used for analysis of mitochondrial characteristics and cell morphology of individual tapetal cells. First, cells of confocal image stacks were segmented manually with the aid of the software ImageJ (National Institutes of Health). Single cell image stacks were rescaled bicubically to fit the dimensions 25 nm × 25 nm × 200 nm required for 3D mitochondrial and cell segmentation. Single image stacks were reprocessed by medium filter (7 × 7 neighborhood). If image stacks were too noisy, the image stacks were submitted for 3D Gaussian filtering (5 × 5 × 5 neighborhood, $\sigma = 1$) for noise removal. For segmentation of cells, the cell channels of image stacks were submitted for cell segmentation using Otsu's method (Otsu, 1979) plane by plane, and the largest 3D object reconstructed was kept for further extraction of morphological features. Mitochondrial segmentation was accomplished by adaptive local thresholding (Peng et al., 2011) plane by plane and 3D single mitochondrial objects were reconstructed. Objects with sizes <0.05 μm^3 and intensity <0.2 × maximum intensity were removed as noise. Three-dimensional mitochondrial and cell objects were applied for feature extraction and geometric and texture features were extracted. Centroids of mitochondria and cells were further used for calculation of features of mitochondrial distribution, including paired mitochondrial distance, distance of mitochondria to mitochondrial centroid or nuclear centroid, etc. Morphological features of mitochondria were used for classification of the mitochondrial morphological subtypes. Thirteen mitochondrial subtype clusters were identified by unsupervised clustering and *k*-means clustering, and six mitochondrial morphological subtypes were justified, according to the literature regarding correlations of mitochondrial morphology and functions. Six mitochondrial morphological subtypes were used to classify tapetal mitochondria as shown in Figure 8C, including fragmented (blue, <1.9 mm^3), lumps

(yellow, aspect ratio < 2, area > 1.9 mm^3), simple tubules (green, short and not branched), branched tubules (light purple; branch number > 0 but Euler number is 1), small reticulum (gold; Euler number ≤ 0; volume < 137 mm^3), and large reticulum (red; Euler number ≤ 0; volume ≥ 137 mm^3). Volume ratio and number ratio of each mitochondrial subtype was calculated. Three-dimensional mitochondrial and cell features of single cell image stacks of different treatments or strains were submitted for statistical analysis by Student's *t* test (2-tail, unpaired) and for features with statistical significance ($P < 0.05$).

Nile Red Staining

To detect neutral lipids on pollen, mature pollen was collected from 10 wild-type and *elm1* flowers infiltrated in 25% glycerol, vortexed for 1 min, and centrifuged at 500*g* for 5 min. After removing flowers, collected pollen was stained with 3.14 μM of Nile Red (cat. no. N3013; Sigma-Aldrich) for 20 min. Single optical sections of pollen were photographed by a model no. LSM 780 confocal microscope using 561-nm/636-nm excitation/emission with an 63×/1.4 oil objective (Leica).

Cryo-SEM

Stamens were dissected from multiple mature buds of wild-type plants, *elm1* and *drp3b* mutants, and loaded on a stub. The samples were frozen by liquid N slush, and then transferred to a sample preparation chamber at −160°C. After 5 min, the temperature was raised to −85°C and sublimed for 15 min. After coating with Pt at −130°C, the samples were transferred to the cryo stage in the SEM chamber and observed at −160°C using a cryo-SEM (Quanta 200 SEM/Quorum Cryo System PP2000TR; FEI) with 20 KV.

Measurement of ATP Content in Mature Pollen

Freshly opened flowers were collected from wild-type and *elm1* mutant in pollen suspension buffer containing 50 mM of K_2HPO_4, and 1% Suc and 4% sorbitol at pH 5.8 (Bernard et al., 2011), and vortexed vigorously. One-hundred microliters of pollen suspension was used for intracellular ATP measurement and protein quantification. For intracellular ATP measurement, 100 μL of pollen suspension was treated with 400 μL of 7% $HClO_4$ and 10 mM of EDTA mixture and incubated for 15 min on ice, then mixed with 100 μL of 5 M KOH and 1 M of triethanolamine mixture for 10 min on ice. The 10-μL supernatant was diluted with 50 mM of Tris (pH 8) after 10,000*g* centrifugation. ATP was measured by ENLITEN rLuciferase/Luciferin reagent (Promega), according to the manufacturer's instructions. Luminescence was quantified using a SpectraMax i3X (Molecular Devices), and 10-s relative light unit integration time was used.

Statistical Analysis

The data were submitted to Student's *t* test for statistically significant difference ($P < 0.05$). Results are shown as mean ± SE with at least three biological replicates.

Accession Numbers

Sequence data from this article can be found in the GenBank/EMBL data libraries under accession numbers: AT5G22350 (ELM1), AT4G33650 (DRP3A), AT2G14120 (DRP3B), AT5G62080 (Lipid transfer protein).

Supplemental Data

The following supplemental materials are available.

Supplemental Figure S1. Alexander staining of wild-type, *drp3a*, and *drp3b* pollen under normal and low light conditions.

Supplemental Figure S2. The production of viable pollen in wild-type (WT), *elm1*, and complement (*Comp.*) lines.

Supplemental Figure S3. TEM images showing mitochondrial morphology in pollen of wild type and mutants.

Supplemental Figure S4. TEM images showing mitochondrial morphology in the tapetum of wild type and *drp3b*.

Supplemental Figure S5. ATP content in wild-type and *elm1* mature pollen.

Supplemental Figure S6. Colocalization of mito-GFP with MitoTracker red in tapetal mitochondria.

Supplemental Figure S7. Correlation of bud size, anther, and pollen in Arabidopsis.

Supplemental Figure S8. Percentage of six mitochondrial subtypes in wild-type tapetum at different developmental stages.

Supplemental Figure S9. Mitochondrial morphology in wild-type and mutant tapetum at the tetrad to the VP stages.

Supplemental Movie S1. 3D Mitochondria in a tetrad-stage tapetal cell.

Supplemental Movie S2. 3D PI-staining image of a tetrad-stage tapetal cell.

ACKNOWLEDGMENTS

The authors thank Dr. Shin-Ichi Arimura (University of Tokyo) for providing *elm1* complement lines; Dr. Anthony Huang (University of California, Riverside) and Dr. Ming-Der Huang (National Sun Yat-Sen University, Taiwan) for providing the tapetum-specific promoter; Dr. Andreas Nebenführ (University of Tennessee) for mito-GFP plasmid; Ms. Shu-Chen Shen (Division of the Instrument Service, Academia Sinica) for assistance in the use of the confocal microscope; the Live-Cell-Imaging Core Lab and the Plant Cell Biology Core Lab at the Institute of Plant and Microbial Biology at Academia Sinica for technical support and equipment; and the Arabidopsis Biological Resource Center for providing transfer DNA mutant lines. We thank Academia Sinica, Taiwan and The Ministry of Science Technology, Taiwan for funding support.

Received February 15, 2019; accepted February 27, 2019; published March 21, 2019.

LITERATURE CITED

Ariizumi T, Toriyama K (2011) Genetic regulation of sporopollenin synthesis and pollen exine development. Ann Rev Plant Biol **62:** 437–460

Arimura SI (2018) Fission and fusion of plant mitochondria, and genome maintenance. Plant Physiol **176:** 152–161

Arimura S, Tsutsumi N (2002) A dynamin-like protein (ADL2b), rather than FtsZ, is involved in Arabidopsis mitochondrial division. Proc Natl Acad Sci USA **99:** 5727–5731

Arimura S, Aida GP, Fujimoto M, Nakazono M, Tsutsumi N (2004) Arabidopsis dynamin-like protein 2a (ADL2a), like ADL2b, is involved in plant mitochondrial division. Plant Cell Physiol **45:** 236–242

Arimura S, Fujimoto M, Doniwa Y, Kadoya N, Nakazono M, Sakamoto W, Tsutsumi N (2008) Arabidopsis ELONGATED MITOCHONDRIA1 is required for localization of DYNAMIN-RELATED PROTEIN3A to mitochondrial fission sites. Plant Cell **20:** 1555–1566

Arimura SI, Kurisu R, Sugaya H, Kadoya N, Tsutsumi N (2017) Cold treatment induces transient mitochondrial fragmentation in *Arabidopsis thaliana* in a way that requires DRP3A but not ELM1 or an ELM1-like homologue, ELM2. Int J Mol Sci **18:** 2161

Arnoult D (2007) Mitochondrial fragmentation in apoptosis. Trends Cell Biol **17:** 6–12

Aung K, Hu J (2012) Differential roles of Arabidopsis dynamin-related proteins DRP3A, DRP3B, and DRP5B in organelle division. J Integr Plant Biol **54:** 921–931

Balk J, Leaver CJ (2001) The PET1-CMS mitochondrial mutation in sunflower is associated with premature programmed cell death and cytochrome *c* release. Plant Cell **13:** 1803–1818

Bernard C, Traub M, Kunz HH, Hach S, Trentmann O, Möhlmann T (2011) Equilibrative nucleoside transporter 1 (ENT1) is critical for pollen germination and vegetative growth in Arabidopsis. J Exp Bot **62:** 4627–4637

Buchanan BB, Grulssem W, Jones RL, Bewley JD, Hempel FD, McCormick S, Zambryski P, eds (2000) Biochemistry and Molecular Biology of Plants. American Society for Plant Physiology, Rockville, MD

Cai Q, Guo L, Shen Z-R, Wang D-Y, Zhang Q, Sodmergen (2015) Elevation of pollen mitochondrial DNA copy number by WHIRLY2: Altered

respiration and pollen tube growth in Arabidopsis. Plant Physiol **169:** 660–673

Chen WW, Freinkman E, Wang T, Birsoy K, Sabatini DM (2016) Absolute quantification of matrix metabolites reveals the dynamics of mitochondrial metabolism. Cell **166:** 1324–1337.e11

Chen X, Zhang H, Sun H, Luo H, Zhao L, Dong Z, Yan S, Zhao C, Liu R, Xu C, et al (2017) IRREGULAR POLLEN EXINE1 is a novel factor in anther cuticle and pollen exine formation. Plant Physiol **173:** 307–325

Crompton M (1999) The mitochondrial permeability transition pore and its role in cell death. Biochem J **341:** 233–249

Dong C, Fu Y, Liu G, Liu H (2014) Low light intensity effects on the growth, photosynthetic characteristics, antioxidant capacity, yield and quality of wheat (*Triticum aestivum* L.) at different growth stages in BLSS. Adv Space Res **53:** 1557–1566

Fujimoto M, Arimura S, Mano S, Kondo M, Saito C, Ueda T, Nakazono M, Nakano A, Nishimura M, Tsutsumi N (2009) Arabidopsis dynamin-related proteins DRP3A and DRP3B are functionally redundant in mitochondrial fission, but have distinct roles in peroxisomal fission. Plant J **58:** 388–400

Green DR, Reed JC (1998) Mitochondria and apoptosis. Science **281:** 1309–1312

Grienenberger E, Kim SS, Lallemand B, Geoffroy P, Heintz D, Souza CdeA, Heitz T, Douglas CJ, Legrand M (2010) Analysis of TETRAKETIDE α-PYRONE REDUCTASE function in *Arabidopsis thaliana* reveals a previously unknown, but conserved, biochemical pathway in sporopollenin monomer biosynthesis. Plant Cell **22:** 4067–4083

Gu JN, Zhu J, Yu Y, Teng XD, Lou Y, Xu XF, Liu JL, Yang, ZN (2014) DYT1 directly regulates the expression of TDF1 for tapetum development and pollen wall formation in Arabidopsis. Plant J **80:** 1005–1013

Hsieh K, Huang AH (2005) Lipid-rich tapetosomes in Brassica tapetum are composed of oleosin-coated oil droplets and vesicles, both assembled in and then detached from the endoplasmic reticulum. Plant J **43:** 889–899

Hsieh K, Huang AH (2007) Tapetosomes in Brassica tapetum accumulate endoplasmic reticulum-derived flavonoids and alkanes for delivery to the pollen surface. Plant Cell **19:** 582–596

Hu J, Huang W, Huang Q, Qin X, Yu C, Wang L, Li S, Zhu R, Zhu Y (2014) Mitochondria and cytoplasmic male sterility in plants. Mitochondrion **19:** 282–288

Huang MD, Chen TL, Huang AH (2013) Abundant type III lipid transfer proteins in Arabidopsis tapetum are secreted to the locule and become a constituent of the pollen exine. Plant Physiol **163:** 1218–1229

Kim SS, Grienenberger E, Lallemand B, Colpitts CC, Kim SY, Souza CdeA, Geoffroy P, Heintz D, Krahn D, Kaiser M, et al (2010) LAP6/POLYKETIDE SYNTHASE A and LAP5/POLYKETIDE SYNTHASE B encode hydroxyalkyl α-pyrone synthases required for pollen development and sporopollenin biosynthesis in *Arabidopsis thaliana*. Plant Cell **22:** 4045–4066

Lee SL, Warmke H (1979) Organelle size and number in fertile and cytoplasmic male-sterile corn. Am J Bot **66:** 141–148

Li Y, Suen DF, Huang CY, Kung SY, Huang AH (2012) The maize tapetum employs diverse mechanisms to synthesize and store proteins and flavonoids and transfer them to the pollen surface. Plant Physiol **158:** 1548–1561

Logan DC (2010) Mitochondrial fusion, division and positioning in plants. Biochem Soc Trans **38:** 789–795

Logan DC, Scott I, Tobin AK (2003) The genetic control of plant mitochondrial morphology and dynamics. Plant J **36:** 500–509

Logan DC, Scott I, Tobin AK (2004) ADL2a, like ADL2b, is involved in the control of higher plant mitochondrial morphology. J Exp Bot **55:** 783–785

Luo D, Xu H, Liu Z, Guo J, Li H, Chen L, Fang C, Zhang Q, Bai M, Yao N, et al (2013) A detrimental mitochondrial-nuclear interaction causes cytoplasmic male sterility in rice. Nat Genet **45:** 573–577

Mano S, Nakamori C, Kondo M, Hayashi M, Nishimura M (2004) An Arabidopsis dynamin-related protein, DRP3A, controls both peroxisomal and mitochondrial division. Plant J **38:** 487–498

Mishra P, Chan DC (2016) Metabolic regulation of mitochondrial dynamics. J Cell Biol **212:** 379–387

Nelson BK, Cai X, Nebenführ A (2007) A multicolored set of in vivo organelle markers for co-localization studies in Arabidopsis and other plants. Plant J **51:** 1126–1136

Otsu N (1979) A threshold selection method from gray-level histograms. IEEE Trans Syst Man Cybern **9:** 62–66

Owen HA, Makaroff CA (1995) Ultrastructure of microsporogenesis and microgametogenesis in *Arabidopsis thaliana* (L.) Heynh. ecotype *Wassilewskija* (Brassicaceae). Protoplasma **185:** 7–21

Papini A, Mosti S, Brighigna L (1999) Programmed-cell–death events during tapetum development of angiosperms. Protoplasma **207:** 213–221

Peng JY, Lin CC, Chen YJ, Kao LS, Liu YC, Chou CC, Huang YH, Chang FR, Wu YC, Tsai YS, et al (2011) Automatic morphological subtyping reveals new roles of caspases in mitochondrial dynamics. PLOS Comput Biol **7:** e1002212

Phan HA, Iacuone S, Li SF, Parish RW (2011) The MYB80 transcription factor is required for pollen development and the regulation of tapetal programmed cell death in *Arabidopsis thaliana*. Plant Cell **23:** 2209–2224

Quilichini TD, Friedmann MC, Samuels AL, Douglas CJ (2010) ATP-binding cassette transporter G26 is required for male fertility and pollen exine formation in Arabidopsis. Plant Physiol **154:** 678–690

Quilichini TD, Douglas CJ, Samuels AL (2014) New views of tapetum ultrastructure and pollen exine development in *Arabidopsis thaliana*. Ann Bot **114:** 1189–1201

Rose RJ, Sheahan MB (2012) Plant mitochondria. eLS doi: 10.1002/9780470015902.a0001680.pub2

Sanders PM, Bui AQ, Weterings K, McIntire KN, Hsu Y-C, Lee PY, Truong MT, Beals TP, Goldberg RB (1999) Anther developmental defects in *Arabidopsis thaliana* male-sterile mutants. Sex Plant Reprod **11:** 297–322

Scott I, Logan DC (2011) Mitochondrial dynamics. *In* F Kempken, ed, Plant Mitochondria. Springer, New York, NY, pp 31–63

Scott I, Tobin AK, Logan DC (2006) BIGYIN, an orthologue of human and yeast FIS1 genes functions in the control of mitochondrial size and number in *Arabidopsis thaliana*. J Exp Bot **57:** 1275–1280

Shi J, Tan H, Yu XH, Liu Y, Liang W, Ranathunge K, Franke RB, Schreiber L, Wang Y, Kai G, et al (2011) Defective pollen wall is required for anther and microspore development in rice and encodes a fatty acyl carrier protein reductase. Plant Cell **23:** 2225–2246

Shi J, Cui M, Yang L, Kim YJ, Zhang D (2015) Genetic and biochemical mechanisms of pollen wall development. Trends Plant Sci **20:** 741–753

Suen DF, Norris KL, Youle RJ (2008) Mitochondrial dynamics and apoptosis. Genes Dev **22:** 1577–1590

Ting JT, Wu SS, Ratnayake C, Huang AH (1998) Constituents of the tapetosomes and elaioplasts in *Brassica campestris* tapetum and their degradation and retention during microsporogenesis. Plant J **16:** 541–551

Vizcay-Barrena G, Wilson ZA (2006) Altered tapetal PCD and pollen wall development in the Arabidopsis ms1 mutant. J Exp Bot **57:** 2709–2717

Wu SS, Platt KA, Ratnayake C, Wang TW, Ting JT, Huang AH (1997) Isolation and characterization of neutral-lipid-containing organelles and globuli-filled plastids from *Brassica napus* tapetum. Proc Natl Acad Sci USA **94:** 12711–12716

Wu SS, Moreau RA, Whitaker BD, Huang AH (1999) Steryl esters in the elaioplasts of the tapetum in developing Brassica anthers and their recovery on the pollen surface. Lipids **34:** 517–523

Xu J, Ding Z, Vizcay-Barrena G, Shi J, Liang W, Yuan Z, Werck-Reichhart D, Schreiber L, Wilson ZA, Zhang D (2014) ABORTED MICROSPORES acts as a master regulator of pollen wall formation in Arabidopsis. Plant Cell **26:** 1544–1556

Zhang H, Zhong H, Wang J, Sui X, Xu N (2016) Adaptive changes in chlorophyll content and photosynthetic features to low light in *Physocarpus amurensis* Maxim and *Physocarpus opulifolius* 'Diabolo'. PeerJ **4:** e2125

Zoratti M, Szabò I (1995) The mitochondrial permeability transition. Biochim Biophys Acta Rev Biomembr **1241:** 139–176